COMPARING THE ACIDITIES OF MICROPOROUS ALUMINOSILICATE AND SILICO-ALUMINOPHOSPHATE CATALYSTS: A COMBINED QUANTUM MECHANICS-INTERATOMIC POTENTIAL FUNCTION STUDY

Joachim SAUER[1], Klaus-Peter SCHRODER and Volker TERMATH

Humboldt-Universitat, Institut fur Chemie, Arbeitsgruppe Quantenchemie, Jagerstrasse 10–11, D-10117 Berlin, Germany; e-mail: [1] js@qc.ag-berlin.mpg.de

Received June 18, 1998
Accepted June 22, 1998

Dedicated to Professor Rudolf Zahradnik on the occasion of his 70th birthday.

DFT-B3LYP calculations are performed on 4-ring models of aluminophosphates (AlPOs) and silico-aluminophosphates (SAPOs). The results are used to fit the parameters of ion pair shell model potential functions. The potentials obtained are tested in lattice energy minimizations for berlinite and the microporous materials AlPO-18, AlPO-40, AlPO-52, and VPI-5. Not only does the potential reproduce the observed structures (average error of the cell constants 1.3%), it also predicts vibrational frequencies over the whole frequency range equally well (maximum deviation 50 cm^{-1}). The potential is used to predict the structures and properties of Brønsted acid sites in an aluminosilicate and a SAPO with the chabazite framework structure (HSSZ-13 and HSAPO-34). A new combined quantum mechanics-intermolecular potential function approach (QM-Pot) is used at the DFT level. Comparison is made with full periodic DFT calculations using plane wave basis sets. The deprotonation energies corrected for systematic errors of the methods used are 1 231–1 235 and 1 261–1 280 kJ/mol for HSSZ-13 and HSAPO-34, respectively. The same acid site has a lower acidity in a SAPO than in an aluminosilicate zeolite of the same structure.

Key words: Aluminosilicate catalysts; Silico-aluminophosphate catalysts; DFT-B3LYP; Ion pair shell model potential; Zeolites; Quantum chemistry; *Ab initio* calculations.

Solid acids such as zeolites and the closely related microporous aluminophosphates are important catalysts with large scale use in petrochemical processes. Zeolites have microporous aluminosilicate frameworks and they become solid acids when protons are present as charge-compensating cations. Formally, the Brønsted acid sites in zeolites, Si–O(H)–Al, are created when in a pure silica framework Si is substituted by Al and a proton is added for charge compensation. Aluminophosphates (AlPOs) are isoelectronic with silica and form the same structure types. For example berlinite is an AlPO with the dense structure of α-quartz and AlPO-18 or VPI-5 are microporous analogues of microporous silica. If in AlPOs a P atom is substituted by an Si atom and a proton is added

for charge compensation, the same type of bridging hydroxyl group is created, Si–O(H)–Al, but in a different environment.

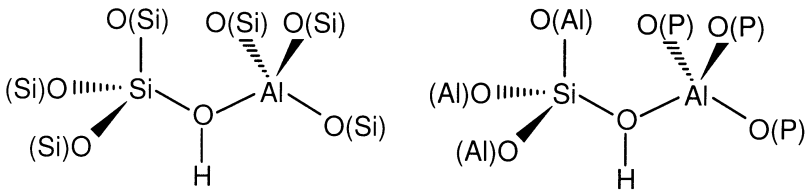

The latter catalysts are silico-aluminophosphates (SAPOs). Understanding the differences in structure and reactivity between zeolites and SAPOs is prerequisite to designing solid acid catalysts. Experimental diffraction methods cannot easily distinguish between Si and Al in zeolites or between P and Si in SAPOs. It is also not easy to determine the intrinsic acidity of surface hydroxyls by experiments because different techniques probe different properties of the acidic site. Therefore, atomistic simulations of the structures of solid acids and quantum mechanical calculations of their intrinsic acidity can significantly contribute to our understanding of this class of important catalysts.

We report here simulation studies on two solid acids with the chabazite (CHA) framework. One is an aluminosilicate, the other one a silico-aluminophosphate. Experimentally, these materials are known as HSSZ-13 and HSAPO-34, respectively. Their structure has been recently examined by neutron diffraction[1,2]. We simulate the structure of these catalysts and predict the crystallographic site where the acidic proton is located. We compare their acidity by calculating the energy of deprotonation of the bridging hydroxyl groups. We use a combined quantum mechanics-interatomic potential function approach for this purpose[3–5]. The active site and its surroundings are treated by density functional theory (DFT) while the periodic lattice is treated by an ion pair shell model potential function. This approach proved very successful for acid zeolite catalysts with different framework structures. Our approach relies on a parametrization of the shell model potential that is based on DFT calculations for cluster models of the materials of interest. DFT-parametrized shell model potentials have been obtained before for aluminosilicates by Sierka and Sauer[6]. Here we report on such potentials for AlPOs and SAPOs. A shell model potential for AlPOs has been derived from experimental data before[7] and, together with a previously derived semiempirical shell model potential for aluminosilicates[8], has been used to simulate SAPOs (ref.[9]). The chabazite framework has been chosen for this pilot study because of its relatively small unit cell size which makes periodic DFT calculations feasible. Comparison will be made with such calculations reported before for HSSZ-13 and HSAPO-34 (refs[10–13]).

A Shell Model Potential for AlPOs and SAPOs Based on DFT Results

Quantum chemical calculations. Three cluster models were chosen for generating data for the parameter fit (Fig. 1). As in previous studies[6,14], ring-type models were favored to minimize the effects of terminating hydroxyl groups. Four- and six-membered rings are also typical building units of microporous AlPOs and SAPOs. The models have the chemical compositions $H_8Al_2P_2O_{12}$ (4R-AlPO), $H_{12}Al_3P_3O_{18}$ (6R-AlPO), and $H_9SiAl_2PO_{12}$ (4R-SAPO). The DFT calculations employed the B3-LYP functional[15,16] and a T(O)DZP basis set[17]. Table I shows details of the optimized structures and the symmetry assumed. Additional data for the fitting procedure were generated by calculating energy gradients for 27 systematically distorted structures of all three models. Bond lengths were changed by 0.05 a.u., angles by 5 degrees.

Parametrization of potential functions. The potential parameters for aluminosilicates generated by Sierka and Sauer[6] were adopted and fixed during the fitting procedure for AlPOs and SAPOs. This way the number of free parameters could be restricted to 12. Oxygen atoms in P–O–Al bridges could not be described by the same parameters as in Si–O–Al bridges. Thus, a new type of oxygen, O_P, was defined in addition to the O and O_b types, defined in the potential for protonated aluminosilicates[6]. Figure 2 shows the definition of atom types for the 4R-SAPO model. Among hydrogen atom types only H_b occurs in periodic calculations on HSAPOs. However, all atom types are needed for free space and embedded cluster calculations.

The fitting procedure was the same as described by Schröder and Sauer[14]. All parameters were obtained in one step. Cartesian gradient components for atoms of terminal hydroxyls were weighted with a factor of 0.1, those of atoms belonging to the ring with a factor of 1. Table II shows the optimized shell model parameters.

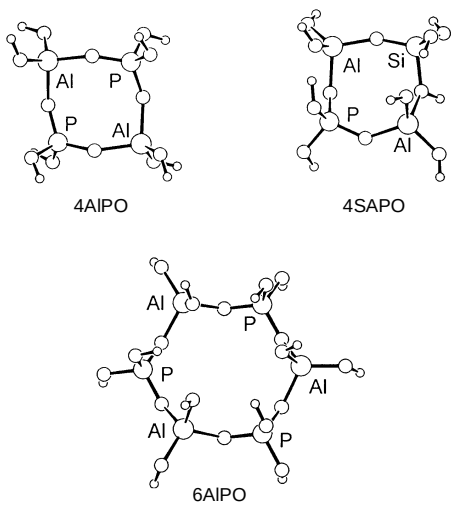

FIG. 1
Ring-type cluster models used in DFT calculations

Results for berlinite and microporous AlPOs. Lattice energy minimizations were performed with the METAPOCS (ref.[18]) and the GULP (ref.[19]) codes. Table III shows calculated cell parameters as well as bond lengths and angles obtained with the DFT potential functions and two predecessors. The first was the rigid ion potential of van Beest *et al.*[20,21]. Its parameters were fitted to Hartree–Fock calculations on $Si(OH)_4$, $Al(OH)_4^-$, and $P(OH)_4^+$. In a second step the parameters were refitted to give better results for α-quartz and berlinite. Gale and Henson[7] fitted the parameters of a shell model potential to observed data for berlinite. Parameters for O–O and Al–O interactions were taken from earlier parametrizations for aluminosilicates[22]. As expected, the experimental berlinite structure[23] is best reproduced by the empirical shell model potential (Table III).

TABLE I
Bond lengths (in pm) and angles (in °) of optimized models obtained by DFT-B3LYP/T(O)DZP calculations

Cluster model	4R-AlPO	6R-AlPO		4R-SAPO	
Point group	D_2	C_{3v}		C_1	
Al–O(–P)	182.5	181.6	183.8, 179.1	Al–O–(–Si)	175.8
P–O(–Al)	152.6	154.2	154.5, 155.9	Al–OH(–Si)	187.9
∠Al–O–P	150.2	134.1	129.8, 137.1	Si–O(–Al)	159.5
∠O–Al–O	100.9–122.6	102.2–115.6	95.8–126.3	Si–OH(–Al)	177.2
∠O–P–O	106.8–118.5	99.9–112.5	104.6–112.4	∠Si–O–Al	155.3
Al–O(–H)	172.5	171.7, 175.5	171.3–178.8	∠Si–O(H)–Al	127.6
(Al–)O–H	96.3	96.2, 96.6	96.2–96.5	∠O–Si–O	102.1–118.5
∠Al–O–H	123.2	118.3, 127.2	122.2–128.5	(Si–)(Al–)O–H	97.4
P–O(–H)	160.8	160.3, 159.1	157.1, 160.4	Si–O(–H)	162.7–164.5
(P–)O–H	97.2	97.2, 98.5	105.3, 97.2	(Si–)O–H	98.6–96.7
∠P–O–H	112.4	100.1–112.3	108.7, 112.3	∠Si–O–H	111.8–115.9

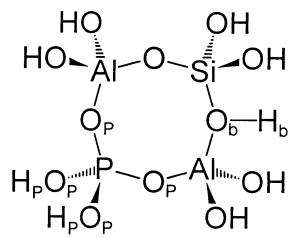

FIG. 2
Definition of atom types shown for the example of the 4R-SAPO model

TABLE II

Parameters of the ion pair shell model potential for SAPOs based on DFT. Only parameters printed in italics were fitted in this work, all others are adopted from Sierka and Sauer[6]

Atom, bond or interaction	Charges[a], *e*		Core-shell interaction
	core + shell	shell	*k*, eV Å^{-2}
O	–2.0[b]	–3.22858	122.47853
O_b	–2.0[b]	–2.81753	70.15123
O_P	–2.0[b]	*–2.92200*	*81.64857*
	short-range repulsion		
	A, eV		*r*, Å
Si–O, Si–O_P	1612.45920		0.29955
Si–O_b	997.88097		0.33212
Al–O	1395.77463		0.30449
Al–O_P	*1109.92381*		*0.31540*
Al–O_b	1644.88177		0.29139
P–O, P–O_P, P–O_b	*1273.42017*		*0.32272*
O_b–H_b	368.64803		0.22511
O–H_b, O_P–H_b	7614.58003		0.19913
O–H	772.06814		0.18524
O_P–H_P	*589.25412*		*0.19666*
O–H_P, O_b–H, O_b–H_P, O_P–H	*80.67811*		*0.38773*
	three-body interaction[c]		
	k[b], eV rad^{-2}		
O–Si–O	0.144703		
O–Si–O_b	0.384711		
O–Al–O	0.893930		
O–Al–O_b	0.686678		
O–Al–O_P, O_b–Al–O_P, O_P–Al–O_P	*0.129982*		
O–P–O	*0.652436*		

[a] Rigid formal charges are assigned to Si(4+), Al(3+), P(5+), and H, H_b, and H_P(1+). [b] Not adjusted. [c] Reference angle θ_0 = 109.47° for all O–T–O angles, not adjusted.

The DFT-parametrized potential of this work predicts too long P–O bonds. This trend is already observed in the quantum mechanical cluster calculations. The potential of van Beest *et al.* provides too large Al–O–P bonding angles. This is not a surprising behaviour for a rigid ion potential.

Table IV shows elastic, dielectric and piezoelectric constants. The values calculated using different potentials are more similar to each other than to the observed ones[24]. In particular the large diagonal terms of the elastic tensor, C_{11} and C_{33}, are not reproduced by the calculations. There is, however, still a large uncertainty in the experimental values. Chang[25] measured $8.58 \cdot 10^{11}$ dyn cm^{-2} for C_{33} – much closer to the values predicted.

Figure 3 shows the vibrational frequencies for the zero wave vector. Comparison with experiment[26] shows the superiority of the DFT-parametrized shell model potential. The largest difference between observed and predicted frequencies is 50 cm^{-1} for this potential, 216 cm^{-1} for the empirical shell model potential, and 125 cm^{-1} for the van Beest potential. The DFT-parametrized potential is accurate over the whole range from 0 to 1 300 cm^{-1}, whereas the empirical shell model shows large deviations for frequencies above 1 000 cm^{-1}.

The crystal structures of $AlPO_4$-18, $AlPO_4$-40, $AlPO_4$-52, and VPI-5 were fully optimized starting from reported X-ray structures[27–30]. The *P*1 space group was assumed. Table V shows the results. The final space groups were identical with the observed ones, with the exception of VPI-5, for which the shell model potentials predict *P*31m rather than the $P6_3$cm. The deviation from observed cell parameters is relatively small. The empirical shell model potential predicts the unit cells best.

TABLE III
Bond lengths (in pm) and angles (in °) in berlinite

Property	Observed[a]	This work	Gale and Henson[b]	van Beest *at al.*[c]
Space group	$P3_12_1$	$P3_12_1$	$P3_12_1$	$P3_12_1$
a	494	502	491	503
c	1 094	1 112	1 096	1 117
Al–O(1)	174	174	174	174
Al–O(2)	173	173	174	174
P–O(1)	152	155	152	150
P–O(2)	152	155	152	151
∠AlO(1)P	142	145	142	150
∠AlO(2)P	143	144	141	151

[a] Ref.[23]. [b] Ref.[7]. [c] Refs[20,21].

TABLE IV
Observed and calculated properties (elastic, dielectric, and piezoelectric constants) of berlinite

Property	Observed[a]	This work	Gale and Henson[b]	van Beest *at al.*[c]
C_{11}, 10^{11} dyn cm^{-1}	6.34	8.25	8.18	8.75
C_{12}, 10^{11} dyn cm^{-1}	0.23	1.31	1.59	1.30
C_{13}, 10^{11} dyn cm^{-1}	0.58	2.08	2.22	1.91
C_{14}, 10^{11} dyn cm^{-1}	–1.21	–1.21	–1.09	–1.24
C_{33}, 10^{11} dyn cm^{-1}	5.58	9.85	10.67	10.40
C_{44}, 10^{11} dyn cm^{-1}	4.32	4.24	4.40	4.88
C_{66}, 10^{11} dyn cm^{-1}	3.06	3.47	3.29	3.74
ε_1^0	5.47	4.22	5.25	1.92
ε_3^0	5.37	4.43	5.42	1.94
ε_1^{hf}	4.60	1.85	2.08	1.00
ε_3^{hf}	4.48	1.87	2.11	1.00
d_{11}, 10^{12} C N^{-1}	–3.30	–2.43	–2.30	–1.57
d_{14}, 10^{12} C N^{-1}	1.62	0.66	1.09	0.24
e_{11}, C m^{-2}	–0.22	–0.36	–0.34	–0.24
e_{14}, C m^{-2}	0.15	0.05	0.08	0.17

[a] Ref.[23]; [b] ref.[7]; [c] refs[20,21].

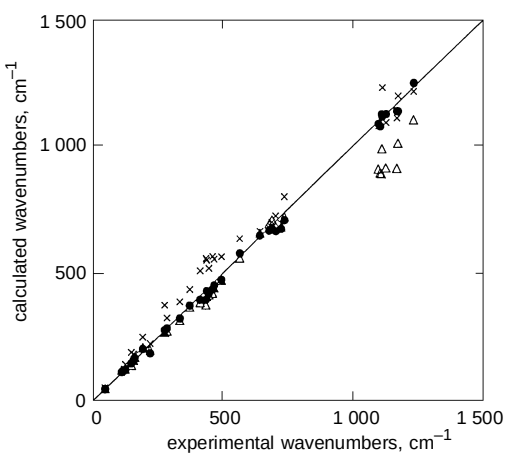

FIG. 3
Calculated *vs* observed vibrational frequencies for berlinite (Δ Gale and Henson, × van Beest *et al.*, ● this work)

Lattice Energy Minimizations Using the DFT-Parametrized Shell Model Potential

Proton siting. First, lattice energy minimizations have been made on HSSZ-13 and HSAPO-34 using the DFT-parametrized shell model potential on unit cells of the composition H-$AlSi_{23}O_{48}$ and H-$SiAl_{12}P_{11}O_{48}$ (Si/Al and Al+P/Si ratios of 23). The crystallographic position into which Al and Si, respectively, are introduced is unique, but the four oxygen positions to which the proton can be attached, O(1) to O(4) are crystallographically different. All four structures are considered. Both the DFT-parametrized and the empirical shell model potential predict O(1)H and O(4)H to be the most stable proton positions in HSAPO-34. Table VI shows the relative stabilities. The CHA framework is built of double-six-membered rings of TO_2 units, which are connected by two oxygen bridges. O(1) is the oxygen linking two six-membered rings within the double-six-ring unit. O(4) belongs to the six-ring and to the 4-ring which is common to two double-six-membered rings. With respect to their position in the double-six-mem-

TABLE V
Observed and calculated unit cell parameters of microporous AlPOs (in pm and in °)

Model		Observed	This work	Gale and Henson[a]	van Beest *et al.*[b]
$AlPO_4$-18		*C*2/*c*	*C*2/*c*	*C*2/*c*	*C*2/*c*
	a	1 371[c]	1 385	1 368	1 396
	b	1 273[c]	1 281	1 261	1 297
	c	1 857[c]	1 872	1 844	1 891
	β	90.01[c]	90.06	90.01	90.03
$AlPO_4$-40		*P*ccn	*P*ccn	*P*ccn	*P*ccn
	a	2 194[d]	2 251	2 217	2 263
	b	1 369[d]	1 392	1 372	1 410
	c	1 425[d]	1 425	1 405	1 435
$AlPO_4$-52		*P*31c	*P*31c	*P*31c	*P*31c
	A	1 372[e]	1 387	1 370	1 406
	C	2 968[e]	2 986	2 924	2 983
VPI-5		$P6_3cm$	*P*31m	*P*31m	$Cmc2_1$
	A	1 852[f]	1 879	1 845	3 310
	B	–	–	–	1 870
	C	833[f]	857	842	848

[a] Ref.[7]; [b] refs[20,21]; [c] ref.[27]; [d] ref.[28]; [e] ref.[29]; [f] ref.[30].

bered ring, O(1) and O(4) correspond to O(1) and O(3), respectively, in the faujasite framework. These are the preferred protonation sites of protonated zeolites with the faujasite structure.

In HSSZ-13 O(1)H is clearly preferred, but O(3)H has about the same stability as O(4)H. The neutron diffraction study localized protons at O(1) and O(3). Hence, it seems that the potential correctly predicts O(1) as the most stable proton site, but that the method is not accurate enough to correctly predict the relative stabilities of the O(3) and O(4) proton. Combined QM-Pot calculations do not change the predicted sequence[31], but a pseudopotential DFT calculation using periodic boundary conditions correctly predicts that O(1) and O(3) are the preferred proton positions.

The neutron diffraction experiment on HSAPO-34 localized one proton at O(2) while the other seems to sit at O(3), a finding at variance with the results of the lattice energy minimizations. It should be noted, however, that the composition of the experimental HSAPO-34 sample[2] is $Si_{2.6}Al_{12}P_{9.4}O_{48}H_{4.3}$. Hence the Al+P/Si ratio of 8 is much smaller than the ratio 23 assumed in the simulation. As a further test we have made combined QM-Pot calculations for O(1)H and O(3)H and found that the former is more stable by 17 kJ/mol.

Structures. Tables VII and VIII show the local structures of the bridging Si–O(H)–Al groups at O(1) and O(4) in HSSZ-13 and HSAPO-34 obtained by lattice energy minimizations using the DFT-parametrized shell model potential. In the Si–O(H)–Al group of the zeolite the Al–O bond (about 190 pm) is much longer than the Si–O bond (about 170 pm). In contrast, for the Si–O(H)–Al group in the SAPO, the two bond

TABLE VI
Relative stabilities (in kJ/mol) of aluminosilicates and silico-aluminiumphosphates protonated at different oxygen sites of the chabasite framework

Method	Material	Ref.	O1	O2	O3	O4
Empirical shell model[a]	HSAPO-34	9	0	14	18	–2
DFT potential	HSSZ-13	31	0	12	5	5
	HSAPO-34	this work	0	13	10	0
QM-Pot	HSSZ-13	31	0	15–21	9–14	3–13
	HSAPO-34	this work	0	–	17	–
Plane wave	HSSZ-13	13	0	7	4	9
	HSAPO-34	13	0	5	2	4
Plane wave	H-SSZ-13	12	0	–	10	–

[a] Includes AlPO-parameters of Gale and Henson[7].

distances are much less different and the Si–O bond (184 pm) is in fact longer than the Al–O bond (180 pm). The OH distance is fairly constant, 97.6 *vs* 97.5 pm for O(1)H, because expansion of the Si–O bond is largely compensated by contraction of the Al–O bond when passing from the zeolite to the SAPO. The empirical shell model potential agrees with the present DFT-parametrized potential on the similar length of the Si–O and Al–O bond, but yields the reverse order.

Combined QM-Pot Calculations

Combined QM-Pot calculations[6] were performed for the O(1)H and the O(4)H groups in HSAPO-34 and for the O(1)H group in H-SSZ-13. Cluster models consisting of two fused 4-rings were embedded in the H-$T_{24}O_{48}$ unit cells (T = Al, P, or Si), see Fig. 4. This $4R^2$-cluster was explicitly treated by the DFT-B3LYP method and the same T(O)DZP basis set was employed as used in the parametrization of the shell model potential.

Bond lengths and angles change by up to 5 pm and 10 degree compared with the results obtained with the shell model potentials alone. The effect that the Si–O bonds become longer and the Al–O bonds shorter when passing from the aluminosilicate to the SAPO is confirmed, although the Al–O bond is slightly longer than the Si–O bond, by about 4 pm, also in SAPO. An increased Si–O bond length is already obtained for the 4R-SAPO cluster. Moreover, the Si–O(H)–Al bond angle becomes significantly narrower and the Si–O–H bond angle significantly wider when passing to the embedded cluster (QM-Pot) approach. As expected, the QM-Pot results are between the lattice energy minimization results using the potential alone and the DFT results on the free space cluster. The non-bond distance between the acidic proton and the Al atom can be deduced from a ^{1}H MAS NMR sideband analysis and a distance of 244 pm was reported for HSAPO-34 (ref.[32]). The distance predicted by our combined QM-Pot method is 245 pm (Table VII).

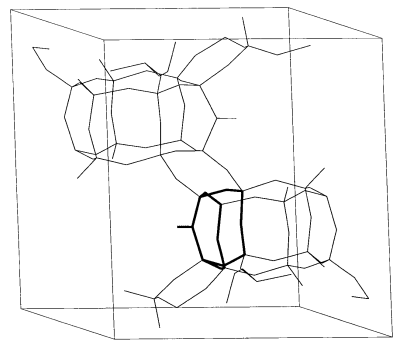

FIG. 4
Unit cell and QM-region ($4R^2$-cluster, bold) for combined QM-Pot calculations

The periodic DFT calculations use a completely different basis set (plane waves together with pseudopotentials) and apply also a different functional. It is therefore not surprising that there are systematic deviations between the plane wave results obtained by Shah *et al.*[13] and the combined QM-Pot results shown in Tables VII and VIII. The largest systematic deviations are found for the Al–O bond length (6 to 7 pm). Nevertheless, the two sets of results agree in all important points: (i) The Si–O and Al–O bonds

TABLE VII
Bond lengths (in pm) and angles (in °) of SiO(H)Al group in HSAPO-34

Bond lengths and angles	Potential and site							
	Empirical potential[a]	DFT		QM-Pot		Cluster (4R-SAPO)	Plane wave[b]	
	O(2)H	O(1)H	O(4)H	O(1)H	O(4)H		O(1)H	O(4)H
Si–O(H)	177	183.5	184.5	179.8	181.2	177.2	176.2	177.7
Al–O(H)	182	179.4	179.7	183.5	184.0	187.9	176.3	177.9
O–H	–	97.5	97.8	97.5	97.8	97.4	97.0	97.0
Al···H	–	237.9	236.5	245.2	244.2	244.1	–	–
∠SiO(H)Al	138.4	137.1	138.7	129.0	130.8	127.6	132.6	131.9
∠SiOH	–	107.4	106.8	112.6	112.2	114.5	110.6	111.0

[a] Ref.[9]; [b] ref.[13].

TABLE VIII
Bond lengths (in ppm) and angles (in °) of the O(1)H group in HSSZ-13, values in parentheses: O(4)H

Bond lengths and angles	DFT potential	QM-Pot	Plane wave[a]
Si–O(H)	169.5 (170.3)	171.7	168.0
Al–O(H)	190.4 (187.5)	191.1	183.8
O–H	97.6 (98.3)	97.7	97.2
Al···H	238.2 (236.1)	245.9	–
∠SiO(H)Al	135.3 (137.5)	129.3	132.8
∠SiOH	107.1 (112.9)	112.7	115.8

[a] Ref.[13].

of the Si–O(H)–Al groups in SAPOs have virtually the same length, whereas in aluminosilicates the Al–O bond is much longer than the Si–O bond. (ii) The Si–O–Al bond angle and the OH bond distance are about the same in aluminosilicates and SAPOs. (iii) The OH bond distance is slightly shorter in SAPOs than in aluminosilicates. In accord with this observation it has been found that the OH vibrational frequencies are slightly higher in SAPOs than in aluminosilicates and it has been concluded that SAPOs may be slightly less acidic than aluminosilicates with the same framework structure[13]. Although a direct relation between the OH bond length or OH vibrational frequency and the acidity cannot be assumed, this conclusion is valid in the present case as will be shown below.

Acidity differences between zeolites and SAPOs. The energy of deprotonation is a measure of the acidity strength of isolated surface hydroxyl groups[5]. Table IX shows the results obtained by different methods for HSSZ-13 and HSAPO-34. All calculations apply a uniform background charge for the anion and an aperiodic correction term[4]. Only the O(1)H group is considered in these calculations. The first conclusion is that a bridging hydroxyl group of a SAPO is less acidic than the crystallographically equivalent hydroxyl group in the aluminosilicate zeolite of the same framework topology. It requires more energy (about 30 kJ/mol) to deprotonate HSAPO-34 than HSSZ-13. In a previous study on different aluminosilicate catalysts with different framework structures a difference of 30 kJ/mol was found between the faujasite and the MFI frameworks[5].

To access further the accuracy of the combined QM-Pot scheme, periodic *ab initio* calculations have been performed which replace the inner shell electrons by pseudopotentials and use plane waves to describe the total periodic wave function of the systems[33]. The Car–Parrinello code[34] was used, for further details see ref.[35]. Due to the lack of exact exchange in these methods a simpler version of DFT, the B-LYP functional without Hartree–Fock exchange was employed and the combined QM-Pot calcu-

TABLE IX
Deprotonation energies of O(1)H groups in HSAPO-34 and HSSZ-13 (in kJ/mol)

Model	DFT parametrized potential	QM-Pot B3LYP[a,b]	QM-Pot BLYP[c]	QM-Pot BLYP[c] corrected[d]	Plane wave B-LYP	Plane wave BLYP corrected[e]
HSSZ-13	1 036	1 231	1 225	1 233	1 197	1 235
HSAPO-34	1 089	1 261	1 272	1 280	1 238	1 276

[a] Correction is about 0 kJ/mol (ref.[6]). [b] 4R[2]-SAPO cluster embedded (Fig. 4). [c] 4R-SAPO cluster embedded. [d] Corrected by an increment of 8 kJ/mol. [e] Corrected by an increment of 38 kJ/mol.

lations have been repeated using this simpler functional. To eliminate the effect of different systematic errors in the different approaches, a constant is added to each of the results which approximately corrects for the systematic errors due to different treatment of electron correlation (B3LYP or BLYP density functionals) and different basis sets. These constants are obtained by calibration calculations of the energy of deprotonation of silanol and methanol, two related molecule for which very accurate values are known[36]. The DFT-B3LYP/T(O)DZP correction happens to be zero (error compensation)[6], while the DFT-BLYP/T(O)DZP correction is 8 kJ/mol. For the plane wave BLYP calculations the correction is 38 kJ/mol. The corrected numbers of the two completely independent approaches, QM-Pot (DFT-BLYP/T(O)DZP) and plane wave (BLYP), are in very good agreement with each other. A similarly good agreement is observed between the two different functionals within the combined QM-Pot approach. Combined QM-Pot calculations have been made before using the Hartree–Fock method instead of DFT calculations and a HF-parametrized shell model potential instead of the DFT-parametrized shell model potential[5]. For the O(1)H group of HSSZ-13 such calculations on an embedded di-tetrahedra cluster yield an uncorrected deprotonation energy of 1 277 kJ/mol. After adding the correction of –46 kJ/mol (ref.[37]) a value of 1 231 kJ/mol is obtained which exactly agrees with the corrected DFT-B3LYP result on the embedded $4R^2$-aluminosilicate cluster. Note that the deprotonation energies presented in Table IX and discussed above do not include zero-point-energy corrections which are about –35 kJ/mol.

Deprotonation energies of surface hydroxyl groups can not be directly measured. However, inferences can be made from OH frequency shifts. Unfortunately, such data are neither available for HSAPO-34 and HSSZ-13, nor for other aluminosilicate–SAPO pair of the same framework topology. Based on temperature programmed desorption of NH_3 and pyridine, Briend *et al.*[38] concluded that "the average strength of the acidity is lower in SAPO-37 than in Y zeolites". It has been shown by QM-Pot calculations that energies of deprotonation and heats of NH_3 adsorption may lead to different relative acidities of two acid zeolites[5]. Hence, we have to await such results for the ammonia adsorption in HSAPO before further conclusions can be reached.

CONCLUSIONS

Parameters of an ion pair shell model potential have been derived from DFT-B3LYP calculations for AlPOs and SAPOs. The potentials obtained are tested for known structures of dense and microporous AlPOs (berlinite, AlPO-18, AlPO-40, AlPO-52, and VPI-5). As expected, the DFT-parametrized shell model potential is slightly inferior to the empirically parametrized one for structures, performs about as well for electric and elastic properties and is clearly superior for vibrational properties.

The SAPO potential is used for describing the periodic SAPO lattice within the new combined quantum mechanics-interatomic potential approach while the cluster embedded into this lattice is explicitly treated by density functional theory (B3LYP) functional.

This approach is used to examine the Brønsted site of an aluminosilicate zeolite, HSSZ13, and of a SAPO, HSAPO-34, both having the chabazite framework structure. Whereas the Si–O and Al–O bond length are different in the different environments, the Si–O(H)–Al bond angle and the OH bond length are very similar.

For the first time explicit comparison is made between the acidities of the two materials, aluminosilicate and SAPO, by calculating the energy of deprotonation. The SAPO is found slightly less acidic. These results are supported by fully periodic DFT calculations using plane wave basis sets and pseudopotentials.

This work has been financially supported by the "Max-Planck-Gesellschaft zur Forderung der Wissenschaften", by the "Deutsche Forschungsgemeinschaft" and by the "Fonds der Chemischen Industrie". We thank Dr M. Sierka and Dr M. Brandle for reading and commenting on the manuscript.

REFERENCES

1. Smith L. J., Davidson A., Cheetham A. K.: *Catal. Lett*. **1997**, *49*, 143.
2. Smith L., Cheetham A. T., Marchese L., Thomas J. M., Wright P. A., Chen J., Gianotti E.: *Catal. Lett*. **1996**, *41*, 13.
3. Eichler U., Kolmel C., Sauer J.: *J. Comput. Chem*. **1997**, *18*, 463.
4. Eichler U., Brandle M., Sauer J.: *J. Phys. Chem. B* **1997**, *101*, 10035.
5. Brandle M., Sauer J.: *J. Am. Chem. Soc*. **1998**, *120*, 1556.
6. Sierka M., Sauer J.: *Faraday Discuss*. **1997**, *106*, 41.
7. Gale J., Henson N. J.: *J. Chem. Soc., Faraday Trans*. **1994**, *90*, 3175.
8. Schroder K.-P., Sauer J., Leslie M., Catlow C. R. A., Thomas J. M.: *Chem. Phys. Lett.* **1992**, *188*, 320.
9. Sastre G., Lewis D. W., Catlow C. R. A.: *J. Phys. Chem. B* **1997**, *101*, 5249.
10. Shah R., Gale J. D., Payne M. C.: *J. Phys. Chem*. **1996**, *100*, 11688.
11. Shah R., Gale J. D., Payne M. C.: *J. Chem. Soc., Chem. Commun*. **1997**, 131.
12. Haase F., Sauer J., Hutter J.: *Chem. Phys. Lett.* **1997**, *266*, 397.
13. Shah R., Gale J. D., Payne M. C.: *Phase Transitions* **1997**, *61*, 67.
14. Schroder K.-P., Sauer J.: *J. Phys. Chem*. **1996**, *100*, 11043.
15. Becke A. D.: *J. Chem. Phys*. **1993**, *98*, 1372.
16. Lee C., Yang W., Parr R. G.: *Phys. Rev. B: Condens. Matter* **1988**, *37*, 785.
17. Schafer A., Horn H., Ahlrichs R.: *J. Chem. Phys*. **1992**, *97*, 2571.
18. Catlow C. R. A., Cormack A. N., Theobald F.: *Acta Crystallogr., Sect. B: Struct. Sci*. **1984**, *40*, 195.
19. Gale J. D.: *J. Chem. Soc., Faraday Trans*. **1997**, *93*, 629.
20. van Beest B. W. H., Kramer G. J., van Santen R. A.: *Phys. Rev. Lett.* **1990**, *64*, 1955.
21. Kramer G. J., Farragher N. P., van Beest B. W. H., van Santen R. A.: *Phys. Rev. B: Condens. Matter* **1991**, *43*, 5068.
22. Jackson R. A., Catlow C. R. A.: *Mol. Simul*. **1988**, *1*, 207.
23. Thong N., Schwarzenbach D.: *Acta Crystallogr., Sect. A: Cryst., Phys., Diffr., Theor. Gen. Crystallogr*. **1979**, *35*, 658.
24. Wang P.-K., Ansermat J.-P., Rudaz S. L., Wang Z., Shore S., Slichter C. P., Sinfield J. H.: *Science* **1986**, *234*, 35.

25. Chang Z. P.: *IEEE Trans. Sonics Ultrasonics* **1976**, *23*, 127.
26. Goullet A., Bretagnon T., Camassel J., Pascual J.: *Phys. Scr.* **1990**, *42*, 478.
27. Simmen A., McCusker L. B., Baerlocher C., Meier W. M.: *Zeolites* **1991**, *11*, 654.
28. McCusker L. B., Baerlocher C.: *Microporous Mater.* **1996**, *6*, 51.
29. McGuire N. K., Bateman C. A., Blackwell C. S., Wilson S. T., Kirchner R. M.: *Zeolites* **1995**, *15*, 460.
30. Annen M. J., Young D., Davis M. E., Cavin O. B., Hubbard C. R.: *J. Phys. Chem.* **1991**, *95*, 1380.
31. Sauer J., Sierka M., Haase F. in: *Modeling the Transition State in Catalysis* (K. Morokuma and D. G. Truhlar, Eds). American Chemical Society, Washington, in press.
32. Hunger M., Anderson M. W., Ojo A., Pfeifer H.: *Microporous Mater.* **1993**, *1*, 17.
33. Galli G., Parrinello M. in: *Computer Simulations in Material Science* (M. Meyer and V. Pontikis, Eds), p. 283. Kluwer, Dordrecht 1991.
34. Hutter J., Ballone P., Bernasconi M., Focher P., Fois E., Goedecker S., Parrinello M., Tuckerman M.: *CPMD 3.0*. Max-Planck-Institut fur Festkorperforschung and IBM Research, Stuttgart 1990–1996.
35. Termath V., Haase F., Sauer J., Hutter J., Parrinello M.: *J. Am. Chem. Soc.*, in press.
36. Sauer J., Ahlrichs R.: *J. Chem. Phys.* **1990**, *93*, 2575.
37. Sauer J. in: *Modelling of Structure and Reactivity in Zeolites* (C. R. A. Catlow, Ed.), p. 183. Academic Press, London 1992.
38. Briend M., Lamy A., Dzwigaj S., Barthomeuf D. in: *Zeolite Chemistry and Catalysis* (P. A. Jacobs, N. I. Jaeger, L. Kubelkova and B. Wichterlova, Eds), Stud. Surf. Sci. Catal., Vol. 69, p. 313. Elsevier, Amsterdam 1991.